AIAA JOURNAL
Vol. 47, No. 6, June 2009

Dynamics of Shock Dispersion and Interactions in Supersonic Freestreams with Counterflowing Jets

Endwell O. Daso,* Victor E. Pritchett,† and Ten-See Wang‡
NASA Marshall Space Flight Center, Huntsville, Alabama 35812
Dale K. Ota§
HyPerComp, Inc., Westlake Village, California 91362
Isaiah M. Blankson¶
NASA John H. Glenn Research Center at Lewis Field, Cleveland, Ohio 44135
and
Aaron H. Auslender**
NASA Langley Research Center, Hampton, Virginia 23681-2199

DOI: 10.2514/1.30084

This study describes an active flow control concept that uses counterflowing jets to significantly modify external flowfields and strongly disperse the shock waves of supersonic and hypersonic vehicles to reduce aerothermal loads and wave drag. The potential aerothermal and aerodynamic benefits of the concepts were investigated by conducting experiments on a 2.6%-scale Apollo capsule model in Mach 3.48 and 4.0 freestreams in a trisonic blowdown wind tunnel, as well as pretest computational fluid dynamics analyses of the flowfields, with and without counterflowing jets. The model employed three sonic and two supersonic (with design Mach numbers of 2.44 and 2.94) jet nozzles with exit diameters ranging from 0.25 to 0.5 in. The schlieren images were consistent with the pretest computational fluid dynamics predictions, showing a long penetration mode jet interaction at low jet flow rates of 0.05 and 0.1 lb_m/s, whereas a short penetration mode jet was revealed at higher flow rates. The long penetration mode jet appeared to be almost fully expanded and was unsteady, with the bow shock becoming so dispersed that it was no longer discernible. High-speed camera schlieren data revealed the bow shock to be dispersed into striations of compression waves, which suddenly coalesced to a weaker bow shock with a larger standoff distance as the flow rate reached a critical value. Heat transfer results showed a significant reduction in heat flux, even giving negative heat flux for some short penetration mode interactions, indicating that the flow wetting the model had a cooling effect, instead of heating, which could significantly impact thermal protection system requirements and design. The findings suggest that high-speed vehicle design and performance can benefit from the application of counterflowing jets as an active flow control.

Nomenclature

D	=	aerodynamic drag, model diameter
D_j	=	counterflowing jet nozzle exit diameter
L	=	aerodynamic lift
M_j	=	counterflowing jet nozzle Mach number
$M1$	=	nozzle Mach number (M_j) of 1 (sonic)
$M2.5$	=	nozzle Mach number (M_j) of 2.44
$M3$	=	nozzle Mach number (M_j) of 2.94
P_o	=	total pressure of counterflowing jet
P_s	=	static pressure of counterflowing jet
Re/l	=	Reynolds number/length
$\dot{q}$	=	heat flux
T_o	=	total temperature of counterflowing jet
T_s	=	static temperature of counterflowing jet
α	=	angle of attack
Δ	=	shock standoff distance

Presented as Paper 1423 at the 45th AIAA Aerospace Sciences Meeting and Exhibit, Reno, NV, 8–11 January 2007; received 28 January 2007; revision received 1 July 2008; accepted for publication 10 July 2008.

*Aerospace Flight Systems. Senior Member AIAA.
†Aerospace Engineer. Member AIAA.
‡Technical Assistant. Senior Member AIAA.
§Member of Technical Staff. Senior Member AIAA.
¶Senior Technologist, Mail Stop 5-9. Associate Fellow AIAA.
**Assistant Head, Hypersonic Airbreathing Propulsion Branch, Mail Stop 168.

I. Introduction

ONE of the many technical challenges in space exploration and interplanetary missions is controlled entry and reentry into planetary and Earth atmospheres. Considerable kinetic energy must be dissipated as a spacecraft decelerates and penetrates the atmosphere. Thus, effective heat load management of stagnation points and acreage heating pose significant risk, especially for human missions.

In atmospheric flight, the efficiency and performance of a vehicle or spacecraft is dictated by the physics of the flowfield about the vehicle. Supersonic and hypersonic vehicle flowfields are characterized by strong shock waves that contribute disproportionately to vehicle drag and aerothermal loads. High vehicle drag and aerothermal loads translate into performance penalties such as aerodynamic performance (lift/drag), stringent thermal protection system (TPS) requirements, vehicle range, weight, and payload mass. TPS design and requirements become increasingly challenging at extreme velocities, for example, Earth's atmospheric reentry from lunar and Mars missions because of the severe heat loads induced. Passive TPS can offer only incremental improvements in material temperature limits to manage aerothermal loads. Other approaches must be sought to better mitigate the harsh aerothermal environments and reduce risks associated with planetary atmospheric entry and reentry.

Therefore, the goal of this study is to gain a better understanding of the flow physics involved through wind-tunnel tests and computational fluid dynamics (CFD) analyses to assess the viability of the concept as an active flow technology, in terms of the

aerothermodynamic effects, potential benefits, and technology readiness level.

II. Background

For more than 50 years, active flow control concepts have been studied as a means to modify or change the external flowfields of transonic, supersonic, and hypersonic vehicles and spacecraft to reduce drag and aerothermal loads, and for spacecraft deceleration. In the 1950s, considerable interest was shown in weakening shock systems using opposing jets [1–6]. Stadler and Inouye [2] showed that opposing jets at low "flow weights" (flow rates) doubled the convective heat transfer to a hemispherical model, whereas heat transfer was reduced by half with tangentially injected jets at equivalent flow weights at the stagnation point. On the other hand, Rashis [3] found considerable surface cooling with counterflowing water jets. Ferri and Bloom [4] performed analyses, using an approximate theory, and tests of upstream water and air injection in a Mach 6.1 freestream for five model shapes, from a sphere-cylinder to cone-cylinders with slightly different heights. They showed that directed upstream fluid injection could be an effective means of cooling in a hypersonic flow and that the theoretical analysis correlated well with air jet cooling on the 50 deg cone model. Resler and Sears [5] explored the use of electromagnetic effects to improve aerodynamic performance. Ziemer [6] demonstrated the effects of magnetic fields on the standoff distance of the bow shock of a sphere in a supersonic stream while showing the shock to be significantly diffused, with an attendant increase in shock standoff distance.

In the 1960s and 1970s, studies were conducted on various flowfield modifications for wave drag and heat load reduction [7–18], using both gas and liquid counterflow or forward-facing jets, including a flight experiment [11] to improve radiowave attenuation to mitigate communications blackout. Warren [7] experimentally studied the effect of ejecting nitrogen and helium gasses upstream into a Mach 5.8 freestream of a sphere-cone model. The coolant gasses effectively reduced heat flux on the model if the freestream was not disturbed by the injected gas (i.e., at low coolant gas flow rates), whereas the coolant effectiveness was considerably reduced at larger flow rates. He noted that a stagnation circle formed on the model with an increase in the heat flux, giving a net heat flux greater with than without injection.

Charczenco and Hennessey [8] used a retrorocket to produce a supersonic counterflowing jet to investigate drag reduction on a sphere model with conical aftbody. They observed flow instability about the nose, with less drag than the case with the retrorocket off, except at very large retrorocket thrust coefficients. Romeo and Sterrett [9,12] investigated the effect of a forward-facing jet on the bow shock of a blunt body in a Mach 6 freestream. They found two modes of shock displacement. In one mode, the blunt body bow shock grew in size but retained its structure. In the second, the shock standoff distance increased considerably, with the shock becoming less steady as the Mach number increased and at high total pressure ratios.

Grimaud and McRee [10] performed a stagnation-point gas injection experiment on a hemisphere-cone in a hypersonic arc tunnel. Blunt body heating rates increased initially at lower coolant flow rates, but decreased with increasing flow rate, with up to a 33% reduction in heat transfer for different coolants at maximum coolant injection rates. Beckwith and Bushnell [11] reported a flight test experiment at 150,000 ft. altitude and velocity of $14,000$ ft/s, using intermittent nose and side port water injections to reduce aerodynamic heating of a sphere-cone having a 9 deg half-angle cone-cylinder flare and a spherical blunt nose (RAM B2). The water injection resulted in a decrease in surface temperatures, ranging from 155 to 408°F, corresponding to heat loads of 240–470 Btu/ft^2 over 90 s. Using a water evaporation theory with their data, they calculated negative surface heat transfer (indicating the cooling effect of pulsed side port injection) that became less negative with distance.

Barber [13] tested the cooling effects of counterflowing stagnation-point injection with nitrogen, helium, and hydrogen on a 90 deg sector copper hemisphere in a Mach 6–8 tunnel with total enthalpies between 1500 and 5000 Btu/lb$_m$. For nitrogen and helium injections, the average heat transfer initially decreased with increasing "relative mass flow," whereas it increased by 10% above the case without injection due to an impinging or reattached "stagnation ring" at a relative mass flow of ~8. With hydrogen injection, the heat transfer increased by 65%, as a result of combustion. However, the average heat transfer decreased considerably as relative mass flow increased, becoming as low as 10% of the case without injection at large relative mass flows for all test gasses.

Finley [14] analytically and experimentally investigated counterflowing jets in a Mach 2.5 freestream using sonic and Mach 2.6 jet nozzles with different diameter ratios. His detailed analysis showed the effects of the jet Mach number and "flow force coefficient" to be critical in determining whether the flow was steady or unsteady. Keyes and Hefner [15] conducted tests with "retropropulsion" as counterflowing jets for spacecraft deceleration in atmospheric decent. Their results showed that aerodynamic drag generally increased with jet total pressure for jets located at the periphery. Bushnell and Huffman [16] studied long penetration mode (LPM) jet interactions and noted that the cooling effects of stagnation-point injection depended upon the water jet's penetration distance. Jarvinen and Adams [17] showed a flowfield with two regimes of jet penetration (long and short penetrations) for a single nozzle retrorocket engine on conical aeroshell planetary entry vehicles. The long penetration jet was seen at low thrusting coefficients, whereas a blunt short jet ending in terminal shock [14] was observed at large coefficients. The transition from long penetration to short penetration occurred at fixed jet exit pressure to freestream pressure ratio for all engine sizes tested.

McGhee [18] also investigated the effects of a centrally located "retronozzle" with an exit Mach number of 3.0 on a 140 deg blunt cone in Mach 3.0, 4.5, and 6.0 freestreams, at 0, 2, and 5 deg angles of attack. Three flow regimes were identified in terms of nozzle expansion. In regime 1, the jet was overexpanded, with local flow static pressure greater than jet exit pressure. In regime 2, the jet was fully expanded, with static pressure approximately equal to the jet exit pressure. In regime 3, the jet was under-expanded, with static pressure less than jet exit pressure. The flowfield was unsteady in regimes 1 and 2, but steady at all angles of attack in regime 3. In the steady flow regime, the locations of the jet (barrel) shock, flow interface, and bow shock were found to be primarily a function of nozzle thrust coefficient. Grenich and Woods [19] demonstrated a concept for heat load and drag reduction on ballutes in a Mach 20 freestream, identifying steady and unsteady flows for low and high jet flow rates [18], respectively. Their results [19] showed a significant reduction in drag coefficient on the ballute as a function of flow rate.

In recent years, there has been strong interest in using weakly ionized nonequilibrium plasma (WINP) jets to reduce wave drag and heat flux of bodies in supersonic and hypersonic flows. More recent works [20–40] have revealed that various shock-dissipating and anomalous effects are produced by WINP jets in high-speed flows. Malmuth et al. [34] and Formin et al. [35] studied jet penetrations in plasma jet experiments with truncated cone-cylinder models in Mach 2, 2.5, and 4 supersonic freestreams. These experiments also revealed short penetration mode (SPM) and LPM jets, consistent with previous findings [17,18], with LPM jets giving larger drag reductions and shock standoff distances.

Shang et al. [36–38] and Shang [39] experimentally and computationally investigated the aerodynamic effects of various counterflowing jets, with and without plasma, to determine the amount of drag reduction in a hypersonic flow over a sphere. They reported that jet penetration has two stability modes: an unsteady oscillatory motion under a subcritical state and a nearly steady supercritical state beyond the shock bifurcation point, depending upon the jet's driving stagnation pressure and mass flow rate. Drag reduction was found to depend strongly upon the jet mass flow rate, in agreement with previous work, and had the same trend with and without plasma. However, the plasma jet reduced drag by an additional amount of ~10% [39], which was attributed to the thermal energy deposited by

the plasma. Josyula et al. [40] investigated the application of counterflowing jets for drag reduction in high-speed systems, concluding that it is best suited for hypersonic blunt-nosed bodies.

Gilinsky et al. [41] conducted experiments and CFD analysis to modify the shock wave of cylindrical and butt-end blunt bodies in subsonic and supersonic flows, using single and multiple needles and opposing liquid jets. Their results showed significant reductions in drag, with the drag coefficient decreasing with flow rate. Daso et al. [42] obtained a CFD solution for the SPM jet, giving a drag reduction of more than 15%, including the jet thrust, for a sonic counterflowing jet of a truncated cone-cylinder in a Mach 2 freestream, and developed an analytical approach to predict a sustained LPM jet. Woods et al. [43] showed the effect of counterflowing water jets in a Mach 6 freestream, with the bow shock on a sphere-cylinder transformed into a long oblique shock. Hayashi et al. [44] conducted experimental and numerical studies of opposing jets in a supersonic flow over a sphere-cylinder for thermal protection. Their results also showed significant reductions in drag and heat transfer, and identified steady regime and unsteady flows with shock oscillations, depending upon the jet-to-freestream stagnation pressure ratio.

The preceding literature review shows that an extensive body of work exists on the use of counterflowing or opposing jets to modify supersonic and hypersonic flows for shock dispersion and drag and heat transfer reductions. However, nearly all previous work used model geometries that were sphere-cylinders, sphere-cones, cylinders, (truncated) cone-cylinders, or simple aeroshells. Thus, very little work exists in which more representative models of actual spacecraft configurations, such as reentry vehicles, had been used.

In this work, we experimentally and numerically investigate the flow environment of supersonic freestream-counterflowing jet interactions, and the attendant aerodynamic and aerothermal effects on an actual spacecraft model, a 2.6%-scale Apollo capsule. The counterflowing jets used in this study involve cold jets only, and therefore does not include weakly ionized plasma jets or other plasma effects, though the preceding literature review included plasma jets to cover a more complete body of work. Our goal is to gain a better insight of the flow physics to advance the technology readiness of active flow control as a viable technology for spacecraft and supersonic and hypersonic vehicles, to mitigate aerothermal loads, and to improve lift-to-drag ratio for enhanced aerodynamic performance.

III. Model Geometry and Instrumentation

The test model was a 2.6%-scale Apollo capsule with a diameter of 4 in. It was designed to accommodate five interchangeable counterflowing jet nozzles (Fig. 1). The secondary air supply feedline to the nozzles was housed in the model sting (Fig. 1c). This feedline was a high-pressure tube (5/8 in. outer diameter) welded to the back of the nozzle socket and regulated with a 900-psi valve. A schlieren flow visualization system [45] with low- [standard National Television System Committee (NTSC)] and high-speed cameras was used to capture the flowfield interactions and resulting shock structure and dynamics. The low-speed camera was a Sony DXC-3000A 3CCD color video camera, with the following specifications: fast $f1.4$ medium index prism optics with 250,000 picture sensing elements for a horizontal resolution of over 560 lines, signal-to-noise ratio of 58 dB, geometric distortion of 0%, sensitivity of 2000 lx $f5.6$ at 3200 K (89.9 reflectance), excellent low-light sensitivity of 25 lx minimum illumination ($f1.7$, +18 dB gain up), and a gain of 0, +9, and +18 dB. The high-speed camera was a Fastcam Ranger (Motion Capture Technology's TroubleShooter 1000) with a resolution of 8 pixels in monochrome and 24 bit pixels in color, a shutter speed of up to 20x the recording rate, and a playback rate of up to 1000 frames/s, forward and backward.

Pressure, heat flux, and temperature data were acquired with a Labview data acquisition system. The instrumentation consisted of 56 static pressure ports and 15 Medtherm Schmidt-Boelter heat flux transducers-thermocouples (Model 8-5-0.5-36-SE-20486, with a range of 0–5 $\mathrm{Btu/ft^2s}$ and a calibration uncertainty of ±3% responsivity) on the heat shield and conical aftbody, which was truncated slightly to admit a custom sting. The gauges were installed in a circular pattern consisting of three rows, each with three or more gauges (Fig. 1c).

The model and nozzles were made from 17-4 PH H1050 stainless steel. The nozzles were trapped in a bore in the base, where they were held in place by four jack-on screws. The four diametrically opposite holes for the screws are visible just inside the third array or row of heat flux gauges (Fig. 1c, red circle). At the center of the model is a location mark. This design allowed each nozzle to be readily replaced or interchanged with another from the heat shield or face of the model, without the need to disassemble or remove the model from the sting during testing.

Five nozzles, three sonic and two supersonic (Mach 2.44 and 2.94) nozzles (Fig. 2), were used in the tests. The blank was used as the baseline geometry (no injection). The nozzle exit diameters varied from 0.25 to 0.5 in. to assess the effect of nozzle geometry. The nozzle contours were designed with ADAPT [46], an in-house nozzle design code that used the method of characteristics with boundary-layer displacement thickness correction.

IV. Test Facility

The experimental investigation was conducted in the trisonic wind tunnel (TWT) of the Aerodynamic Research Facility at NASA Marshall Space Flight Center. The TWT is an intermittent blowdown tunnel, with high-pressure air flowing from storage tanks to atmospheric or vacuum conditions. The test section is 21-in. long, with a 14×14 in. cross section, and freestream Mach numbers of 0.2–4.96. A variable diffuser is used to obtain Mach numbers from 0.2 to 1.3, whereas plenum suction and perforated walls are used to achieve transonic Mach numbers from 0.95 to 1.3. A solid wall supersonic test section provides the entire range of Mach numbers from 2.74 to 4.96, using a set of automatically actuated contour nozzle blocks. Angles of attack, from −10 to +10 deg, are provided by a hydraulically controlled pitch sector located downstream of the test section.

For the tests conducted in this study, two freestream Mach numbers, Mach 3.48 and 4.0, were employed for the baseline geometry and counterflowing jet nozzles. Data were not acquired at Mach numbers higher than 4.0 because uniform flow could not be established due to blockage even with the baseline geometry. The nominal tunnel conditions for the Mach 3.48 and 4.0 freestreams were total pressures of 45 and 55 psi, respectively, total temperature of 580°R (140°F), with corresponding unit Reynolds numbers of $4.88 \times 10^6/\mathrm{ft}$ and $4.67 \times 10^6/\mathrm{ft}$.

V. Test Run Matrix

The run matrix included a wide range of jet parameters and the two supersonic freestream Mach numbers of 3.48 and 4.0. Five counterflow jet nozzles (three sonic and two supersonic, with nozzle exit diameters of 0.25, 0.375, and 0.5 in.) were used to assess effects of geometry and Mach number. The nozzles were run at different design flow rates (0.05, 0.10, 0.25, 0.35, and 0.50 lb_m/s) corresponding to the nozzle stagnation pressure and temperatures (Table 1), as well as at three jet angles of attack (5, 0, and −9 deg) to determine the effects of flow rate and angle of attack on the flow structure and interactions. Actual jet flow rates were measured with a turbine-type 5/8-in.-diam volumetric flow meter.

VI. Numerical Simulations

Pretest numerical simulations were performed by HyPerComp, Inc., with an in-house flow solver called USA. The code is a three-dimensional structured-grid, Reynolds-averaged Navier–Stokes equations solver, with perfect gas, finite rate chemistry, equilibrium chemistry, and equilibrium air curve fit options. It has been widely used and validated [47–49].

A computational grid, including the model sting, of ∼750,000 nodes was used to simulate one-half of the computational domain

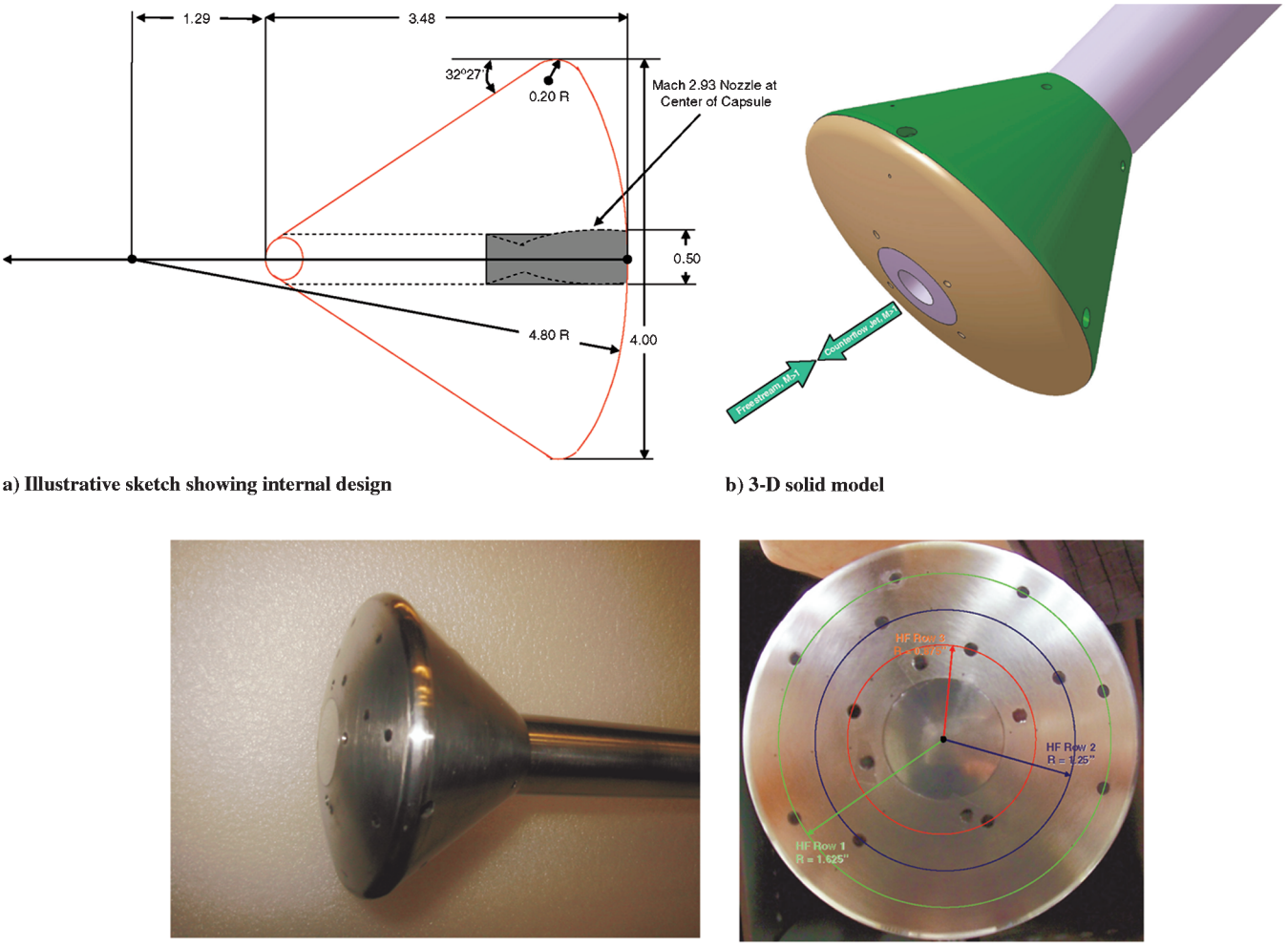

a) Illustrative sketch showing internal design

b) 3-D solid model

c) Model with heat flux (visible) and pressure tap instrumentation

Fig. 1 Model (2.6%-scale) of the Apollo capsule.

(Fig. 3a), with the plane of symmetry at the center of the computational domain ($z = 0$). This arrangement was consistent with the experimental setup, where the center point of the nozzle exit did not move and the capsule rotated about that point. The computational grid consisted of ten zones (Fig. 3a). Zones 1–8 are wraparound grids (rotated around the cylindrical surface), whereas zones 9 and 10 are cylindrical (degenerate) grids. An extensive grid refinement study was conducted to determine grid independence in heat transfer and to resolve the boundary layers, giving a maximum $y^+ < 0.1$, as shown in Table 2 for $M_\infty = 3.48$, $M_j = 2.94$, $D_j = 0.50$. The solutions discussed here were obtained with the perfect gas option of the solver and the pointwise Goldberg one-equation turbulence model.

Figure 3b shows the computational grid of the flowfield with the model and sting at the plane of symmetry and at 10 deg angle of attack, with ~775,000 nodes and two additional zones. This grid was more refined to better resolve regions of high gradients, although the y^+ was about the same as the grid at 0 deg angle of attack. The computational grid of one of the supersonic nozzles is shown in Fig. 4. The single-zone grid was made up of ~25,000 nodes and was only included in the computations for cases with counterflowing jets.

VII. Experimental Results

A. Schlieren Data (Low-Speed Camera)

The discussion of the results focuses on the dynamics of the freestream-counterflowing jet interactions and characteristics of the flow structure. As noted earlier, the test matrix included a wide range of parameters: five jet nozzle geometries (with three sonic jet Mach numbers and two supersonic Mach numbers of 2.44 and 2.94, and three nozzle exit diameters) in addition to the baseline geometry, five different flow rates, and three angles of attack, resulting in nearly 100 runs. The runs were conducted in two sequences for each freestream.

In the first sequence, the flow rate of the counterflowing jet was fixed at a given value. Starting with the lowest flow rate, data were acquired successively for each angle of attack, and then the process

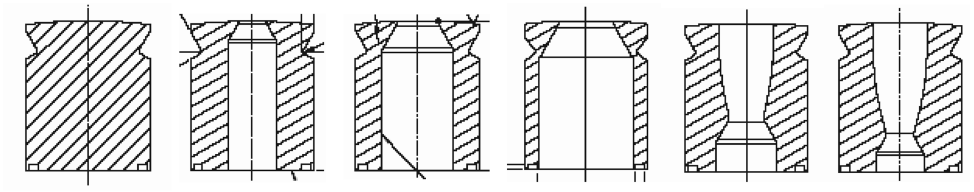

Fig. 2 Sonic and supersonic counterflowing jet nozzles and blank for baseline geometry.

Table 1 Counterflowing nozzle jet flow conditions in tests

Test conditions for $M_\infty = 3.48$, $P_o = 45$ psi, $T_o = 140°$F										
Nozzle diameter, D_j, in.	Design M_j	Design $\dot{m}_j$, lbm/s	Flow meter				Nozzle			
			T_s, °F	P_s, psi	T_o, °R	P_o, psi (calculated)	T_{oj}, °R		P_{oj}, psi	
							Exp.	CFD	Exp.	CFD
0.250	1	0.05	34.0	85.2	496	86.7	496	——	58.7	——
		0.10	23.5	136.7	485	139.1	485	——	95.2	——
		0.35	17.1	431.5	479	439.5	479	——	309.2	——
		0.50	21.5	597.2	484	608.6	484	——	435.7	——
0.375	1	0.05	30.2	66.5	494	68.4	494	——	26.0	——
		0.10	23.5	94.7	487	97.4	487	——	37.7	——
		0.25	16.6	238.0	480	245.5	480	——	99.2	——
		0.35	18.7	311.3	483	321.4	483	——	131.6	——
		0.50	12.3	446.2	476	460.9	476	——	190.4	——
0.500	1	0.05	29.8	56.3	493	57.9	493	540	12.5	11.2
		0.10	23.1	100.2	487	103.2	487	540	22.7	22.5
		0.25	9.6	232.5	473	239.9	473	——	54.8	——
		0.35	11.2	317.2	475	327.6	475	——	75.9	——
		0.50	14.8	428.6	479	443.1	479	540	104.3	111.6
		1.00	——	——	——	——	——	540	——	223.2
0.500	2.44	0.05	34.9	46.1	498	47.2	498	540	24.0	27.9
		0.10	28.9	142.8	492	146.5	492	540	76.1	55.8
		0.25	19.6	235.1	483	241.6	483	——	128.8	——
		0.35	20.9	343.6	484	353.3	484	——	190.6	——
		0.50	24.6	507.7	488	522.5	488	540	285.7	279.0
		1.00	——	——	——	——	——	540	——	557.5
0.500	2.94	0.05	50.3	62.2	512	63.3	512	540	43.6	44.5
		0.10	38.2	131.1	500	133.4	500	540	92.5	89.1
		0.25	21.7	310.3	484	316.1	484	——	223.2	——
		0.35	25.1	429.2	487	437.2	487	——	309.8	——
		0.50	25.1	579.7	487	590.8	487	540	424.2	445.9
		1.00	——	——	——	——	——	540	——	891.9

was repeated for the next flow rate. In the second sequence, for a given run, the flow rate was varied from $\dot{m}_j = 0.05$ to 0.50 lb_m/s for each freestream Mach number at $\alpha = 0$ deg. In addition, some runs were repeated with a higher speed camera (with frame rates of up to 1000 frames/s) in the schlieren system to better capture details of the flow structure for the cases in which the bow shock could not be discerned. Thus, a significant amount of data was acquired. In this paper, we therefore limit the discussion to a representative set of the results for the 0.5-in. nozzle exit diameter jet flowfields, including the effects of the flow rate and jet interaction on heat transfer and shock standoff distance. A more in-depth discussion of the flowfield data, including the effect of nozzle diameter, will be presented in a future paper.

Schlieren images for the Mach 3.48 and 4.0 freestreams are shown in Figs. 5a and 5b, respectively, of the flowfield of the baseline geometry (Fig. 2). These images clearly show the bow shock upstream of the Apollo model, as expected. The light and dark shades are due to the horizontal orientation of the knife edge. A boundary starting from the rim of the model and terminating on the sting, demarcating a pocket of separated flow on the aft-cone, is readily seen. The separated flow results from an adverse pressure gradient on the aft-cone, due to the expansion fan emanating at the edge of the model as the flow accelerates at the rim through the Prandtl–Meyer fan.

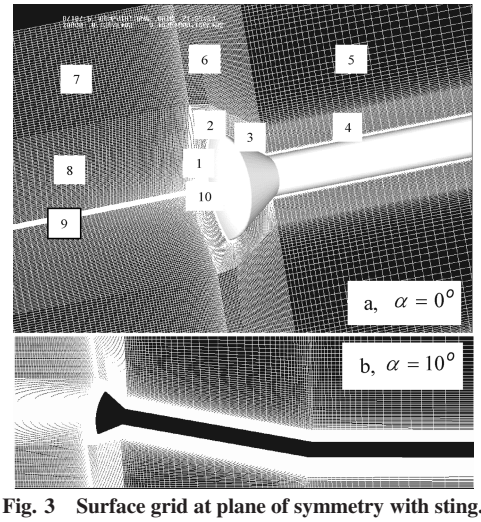

Fig. 3 Surface grid at plane of symmetry with sting.

Figure 6 shows a comparison of the flow structures for the Mach 3.48 freestream for jet with nozzle exit diameters of 0.375 in. (Fig. 6a) and 0.5 in. (Figs. 6b and 6c) at $\alpha = 0$ deg. In the legend, the notation M1-0.375 (Fig. 6a) denotes the jet nozzle design Mach number and exit diameter. M1 indicates a nozzle exit Mach number of 1, whereas the −0.375 represents the nozzle exit diameter of 0.375 in. Similarly, M3 in M3.0-0.5 stands for a design jet Mach number of 2.94 and nozzle diameter of 0.5 in. The mass flow rate $\dot{m}_j$ is denoted by MF. Thus, Fig. 6 shows the effect of the flow rate ($\dot{m}_j = 0.0$ (baseline), 0.05, 0.10, 0.25, 0.35, and 0.50 lb_m/s), Mach number, and nozzle exit diameter.

Figures 6a and 6b show the effect of the nozzle exit diameter on the flow structure. The comparison shows little effect, which may be due to the fact that the difference in the diameters is small. This is also true for the flow structure of the 0.25-in. exit diameter nozzle (not shown). Figures 6b and 6c similarly show the schlieren images for the flowfields with design jet Mach numbers of 1.00 and 2.94, respectively, for the same jet nozzle exit diameter. These images show dramatic differences in the flow structure compared to the baseline. Although different regimes have been identified in previous work, two main flow characteristics are evident in Fig. 6 in terms of the flow structure. In one regime, the counterflowing jet remained essentially a pencil of fluid or an aerospike, penetrating far upstream into the oncoming supersonic freestream, known as a long penetration [17,35,36] mode jet. The other is the short penetration mode jet in which the counterflowing jet exhausts into the freestream with the more familiar plume.

The mode of jet penetration depends upon the flow rate or the driving nozzle stagnation pressure and therefore the type of nozzle

Table 2 Results of grid refinement study for $M_\infty = 3.48$, $M_j = 2.94$, $D_j = 0.50$

Grid no.	No. of grid points	Minimum spacing	y^+_{min}	y^+_{max}	y^+_{avg}	$\dot{q}$
1	398,080	0.001	0.15	7.4	1.4	0.190
2	726,528	0.0001	0.005	0.8	0.14	0.138
3	1.231360×10^6	0.00001	0.0003	0.08	0.014	0.145
4	1.231360×10^6	0.000001	0.00004	0.008	0.0014	0.132

expansion (Fig. 6). That is, whether the jet was underexpanded, fully expanded, or overexpanded, based on the pressure difference between the nozzle exit static pressure and the static pressure of the ambient or shocked flow. At the low flow rates ($\dot{m}_j = 0.05$ and 0.1 lb_m/s), that is, the LPM, the counterflowing jet is seen to be nearly fully expanded, with the static pressure of the jet at the nozzle exit being, by definition, approximately the same as the static pressure of the ambient flow about the nozzle exit, consistent with the result of [18]. Thus, the LPM jet occurred for both the sonic and supersonic nozzles, with the degree of penetration depending upon the jet nozzle exit Mach number (Figs. 6a–6c). For the LPM jet flowfield, the flow structure reveals the shock to be so diffused or dispersed that it was no longer discernible, and thus the shock standoff distance could no longer be defined. To our knowledge, this degree of shock dispersion has only been observed in the schlieren images of McGhee [18], who identified three different flow regimes in the flowfield of a Mach 3 freestream with a 140 deg cone with a centrally located Mach 3 retronozzle at $\alpha = 0$ deg. If it can be sustained, such dispersion or dissipation of the bow shock of the model could have important applications in supersonic and hypersonic aerodynamics.

An equally important characteristic of the flowfields with LPM jets is the rather pronounced unsteadiness of the interactions at low jet flow rates, thrust, or mass flow coefficients [8,9,14,18,19,35,36,44] and oscillation [9,44] through a feedback mechanism. The feedback mechanism is sustained by the mixed hyperbolic-elliptic character of the flowfield. Although a definitive explanation has remained elusive due to the paucity of detailed flowfield measurements, two plausible explanations exist for this self-sustaining unsteadiness and oscillations: they either result from the transitioning of the nozzle wall laminar boundary layer into turbulent fluctuations [9], which promotes mixing as the opposing streams interact, particularly in the case of the supersonic nozzles, or from pressure perturbation in dead-air regions [14] of the flowfield, which propagate upstream due to the adverse pressure gradient. The unsteadiness and oscillations are quite evident in the schlieren videos. Rockwell and Naudascher [50] give an excellent discussion on self-sustained oscillating shear layers, feedback mechanisms, and other characteristic effects. Panaras [51] also discusses pulsating flows in his paper on axisymmetric concave bodies.

For certain types of geometries (spherical-cylinder, sphere-cone, truncated cone-cylinder, and reentry capsule models, as reported here), the basic bow-shock-counterflowing jet flowfield structure is qualitatively similar for the cases with higher jet flow rates (>0.1 lb_m/s). However, at lower flow rates, the degree of shock diffusion reported in this study is known to have been observed in only one previous work [18]. Although spike-tipped blunt bodies and counterflowing jets reduce drag and share some similarities in terms of flow structure, they also have significant differences. These include boundary layers on the aerospikes with large recirculating flow pockets ahead of the blunt body, whereas counterflowing jets produce shear layers instead, which bound a smaller recirculating flow zone adjacent to the blunt body, thus producing different flow characteristics.

Figure 6 also reveals dramatic changes in the flow structure and dynamics of the interaction as the counterflowing jet flow rate was increased above $\dot{m}_j = 0.10$ lb_m/s. For $\dot{m}_j \geq 0.25$ lb_m/s, the flow structure has transitioned from the LPM to the SPM. The schlieren videos show a sudden transition as the LPM jet jumps to SPM at some critical flow rate to instantaneously reestablish a weaker bow shock, with longer standoff distance compared to the baseline and a concomitant reduction in jet penetration. This sudden transition is referred to as bifurcation in some previous work [36]. We have, however, chosen not to identify the transition as bifurcation due to multiple meanings or interpretations of the word in describing other flow phenomena [52].

Figure 7 shows different flow features of the flowfield for SPM jet. In the SPM, the jet is delineated by a barrel shock, capped with a terminal spherical shock downstream of the bow shock, with an interface located about midway from either shock. A supersonic jet stream emanates at the corner where the terminal shock and the jet barrel shock interact, similar to a classical type IV shock interaction [53–56], as seen in Fig. 7. The difference is that, unlike the case of the classical type IV interaction, an isolated shock generator for the incident shock is absent for the freestream-counterflowing jet interaction [51]. The jet stream stagnates or impinges on the surface of the model and forms what Warren [7] called a stagnation circle, giving heat loads greater than the case without injection. The stagnation ring location on the surface moves radially out with increasing flow rate or jet stagnation pressure (Fig. 6). At even higher flow rates, the jet stream is seen to clear the face of the model, relieving the dilemma of increased heating [7]. Also, it is quite noticeable that the pocket of separated flow in the baseline flowfield has disappeared with counterflowing jet injection as a lower pressure region becomes established in the model face.

B. Schlieren Data (High-Speed Camera)

High-speed camera schlieren was used to better capture the details of the flow structure for the flowfield with low jet flow rates ($\dot{m}_j = 0.05$ and 0.10 lb_m/s) in which the bow shock was no longer discernible. These images were taken with a higher resolution camera at speeds of 500 and 1000 frames/s (Figs. 8 and 9). Both

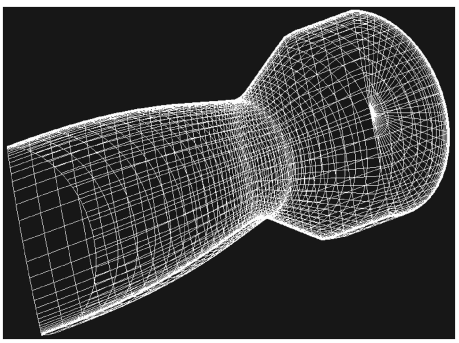

Fig. 4 Mach 2.94 nozzle grid with 0.5-in. exit diameter.

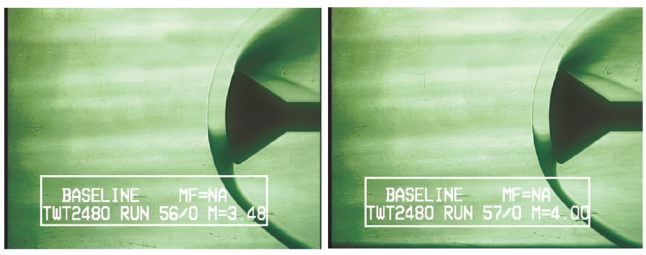

a) $M_\infty = 3.48$ **b) $M_\infty = 4.0$**

Fig. 5 Schlieren images of the flowfield of the baseline geometry with no jet injection.

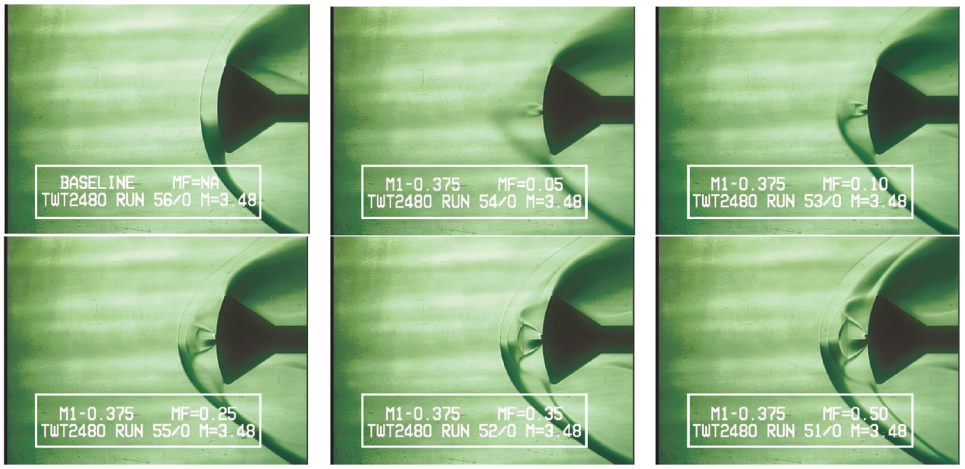

a) Effect of flow rate, MF ($\dot{m}_j$): jet mach number is sonic, nozzle exit diameter = 0.375"

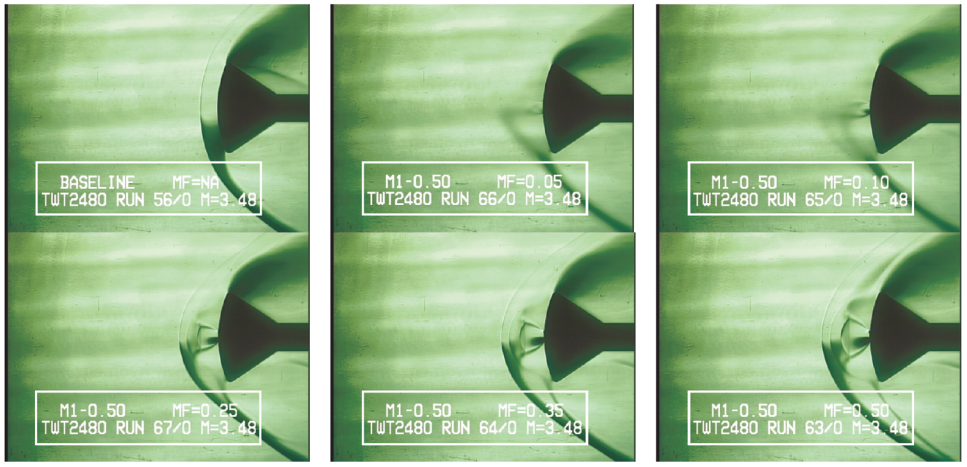

b) Effect of flow rate, MF ($\dot{m}_j$): jet mach number is sonic, nozzle exit diameter = 0.5"

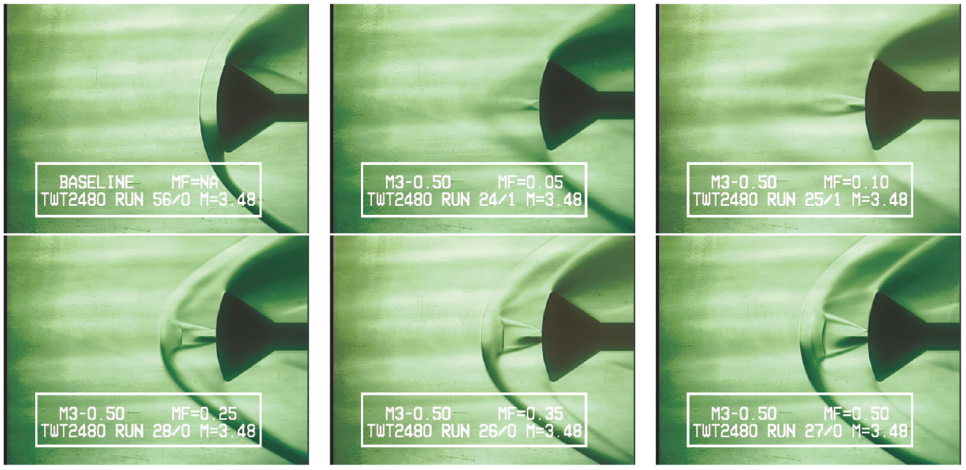

c) Effect of flow rate, MF ($\dot{m}_j$): jet mach number = 2.94, nozzle exit diameter = 0.5"

Fig. 6 Effects of Mach number and flow rate on the interaction of the counterflowing jet with Mach 3.48 freestream.

figures clearly show the dynamics of the supersonic freestream-jet interaction with the sonic and Mach 2.94 counterflowing jets. The images were taken as the flow rate was continuously increased to about 0.25 lb_m/s, with the flow rate increasing from Figs. 8a–8d, and similarly in Fig. 9.

For the interaction with the sonic jet (Fig. 8), the bow shock is seen to be dispersed, with the jet progressively increasing in length upstream as the flow rate was increased incrementally, remaining essentially like a pencil or aerospike, as an LPM jet. The shock is dispersed into striations of compression waves spread over a wide distance, such that a shock standoff distance could no longer be defined in the classical sense. As the flow rate increased further, a critical value was reached at which the compression waves instantaneously coalesced from LPM to the SPM jet, with the sudden reemergence of the bow shock and the flow structure described previously (Fig. 8d). Although not determined during these tests, the critical value was above 0.10 lb_m/s.

Figure 9 shows the schlieren images of the interaction between the supersonic freestream and Mach 2.94 supersonic jet. The dynamics of the dispersion process of the bow shock is the same as those

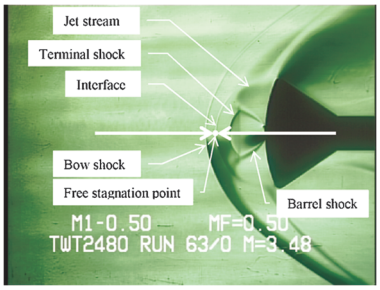

Fig. 7 Characteristic features of the interacting flow structure.

described earlier. The interaction with the supersonic jet reveals even greater flow details of the shock dispersion into compression waves that are quite visible. Gradually increasing the flow rate resulted in an attendant increase in the length of the LPM jet, with the compression waves pushed further upstream, becoming so long that part of the waves were truncated from view. Similarly, above the critical value of the flow rate, the compression waves suddenly coalesced to form the SPM jet, with the reestablishment of the bow shock with longer standoff distance.

The high-speed camera schlieren data reveal details of the dynamics of the bow shock dispersion that gave better insight into the flow physics of the freestream and counterflowing jet interaction. Below the critical flow rate, the dispersion of the shock wave into compression waves suggests three physical processes at play. The first is that the absence of a distinct bow shock nullifies the Rankine–Hugoniot jump conditions, resulting in a recovery in total pressure and compression waves that propagate at speeds higher than the speed of sound. This total pressure recovery promotes or induces the second process, which is a very high rate of mixing of the two opposing streams, with an attendant increase in entropy (mixing, as well as temperature and pressure differences) and becoming a large domain of highly turbulent shear layer. In the third process, as the flow rate was increased above the critical value, the compression waves, with speeds higher than the velocities near the interface, instantaneously coalesced into a new (spherical) bow shock with a standoff distance greater than that of the baseline, which increased with increasing flow rate.

The shock dispersion or diffusion process and sudden transition from LPM to SPM interactions seem to repeat in the opposite sense (that is, from SPM to LPM), reproducing the same flow structure. As noted earlier, the sudden transition from LPM to SPM was readily observable in the schlieren videos, suggesting that the flow

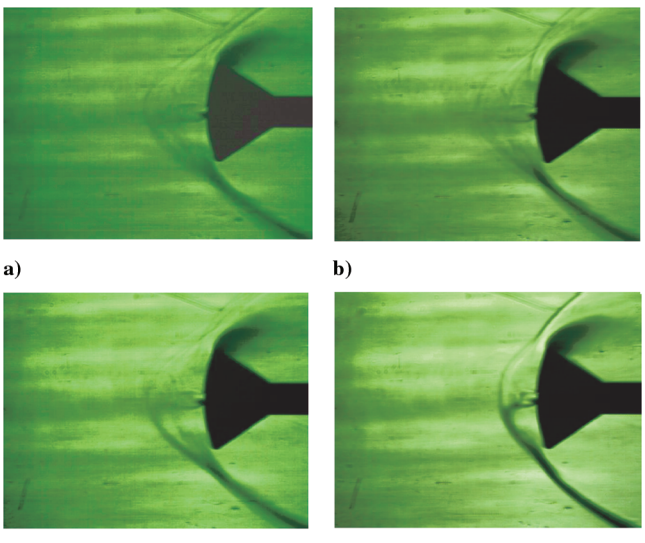

a) **b)**

c) **d)**

Fig. 8 Dispersion of bow shock by counterflowing sonic LPM jet and transition to the SPM jet.

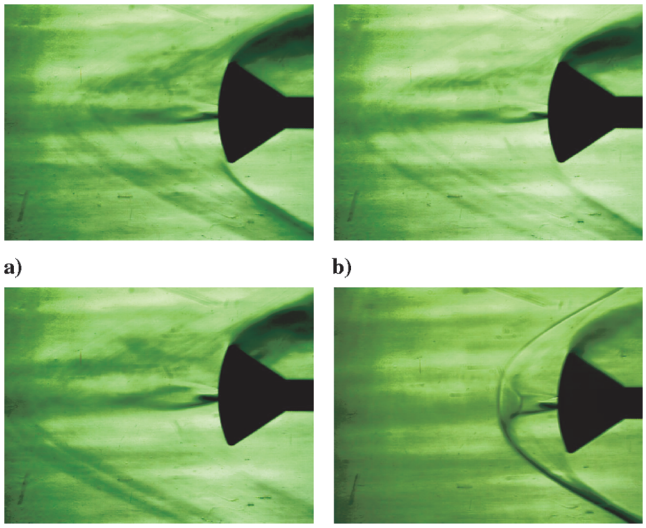

a) **b)**

c) **d)**

Fig. 9 Dispersion of bow shock by counterflowing Mach 2.94 LPM jet and transition to the SPM jet.

phenomena can be controlled to have the desired effects in terms of active flow control for thermal management and better aerodynamic performance. This possibility has two immediate implications as a potential technology. At supersonic speeds, the shock could be so diffused that the formation of an "N" wave could be mitigated to weaken sonic booms, as long as the jet flow rate is not increased to reestablish strong shocks (Figs. 6, 8, and 9). For hypersonic blunt body flows, such as the Apollo capsule or the new crew exploration vehicle (CEV or Orion), the entropy layer would be dissipated in the absence of the strong bow shock, with significant aerothermodynamic implications.

In this paper, shock dispersion or diffusion is used to mean the spreading of the (bow) shock, as seen in the low-speed camera schlieren images (Fig. 6) at the jet flow rates ($\dot{m}_j = 0.05$ and 0.1 lb_m/s) and revealed in greater detail in the high-speed camera (Figs. 8 and 9). It is not used to mean shock attenuation which involves the time decay of shock strength or intensity through shock reflection and/or transmission by other means [57,58].

C. Effects of Angle of Attack

Effects of angle of attack on the flowfield for the interaction between the Mach 4.0 freestream and the Mach 2.94 counterflowing jet ($\dot{m}_j = 0.10$, 0.25, 0.35, and 0.50 lb_m/s) are shown in Fig. 10. These images were taken with the low-speed camera (standard NTSC) schlieren system. Even at $\alpha = -9$ deg, the flow structure of the LPM jet ($\dot{m}_j = 0.10$ lb_m/s) is very much sustained in terms of jet penetration and shock dispersion, although a strong flow asymmetry was introduced, as would be expected. This asymmetry persisted and apparently became stronger with increasing flow rate. However, effects of the angle of attack did not seem to severely diminish the capacity of the counterflowing jets for active flow control, at least at small angles. In the $\alpha = 0$ deg cases, the supersonic jet stream emanating from the interaction of the jet barrel and terminal shocks no longer impinged upon the model [7], as seen in Figs. 10e–10h.

The normalized heat transfer data on the face or heat shield of the model for the interaction of the Mach 3.48 and Mach 4.0 freestreams and the 0.5-in.-diam nozzles with design Mach numbers of 1.0, 2.44, and 2.94 are plotted in Figs. 11 and 12, respectively, and compared with the data for the baseline ($\dot{m}_j = 0.0$ lb_m/s) for $\alpha = 0$ deg. The data are given for each circle or row of heat flux/temperature gauges (Fig. 1c), and each data point on the plot represents the data from each gauge in the row, normalized by the baseline (no jet) value of that gauge. Even at $\alpha = 0$ deg, the data on a given row are not the same and therefore not coincident, which suggests some asymmetry in the flowfield due to unsteadiness, even in the case of the SPM jets. The

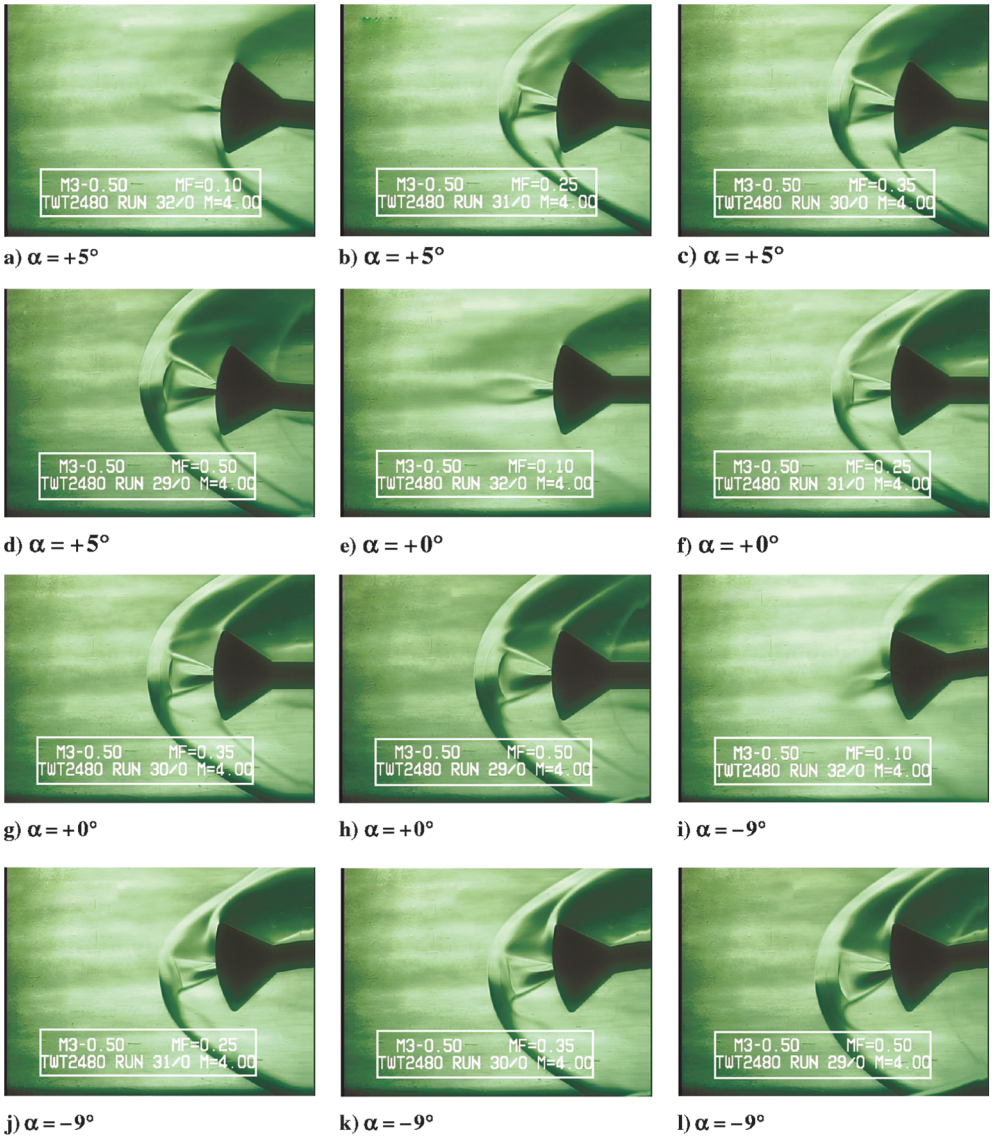

Fig. 10 Effects of angle of attack and flow rate on the interaction of the counterflowing jet with Mach 4.0 freestream.

Mach 3.48 and Mach 4.0 freestreams (Figs. 11 and 12, respectively) both consistently show a dramatic decrease in the heat flux compared with that of the baseline for all design jet nozzle exit Mach numbers. However, near the rim of the model (row 1: $R = 1.625$ in.) the data are higher than the baseline value, with the value for the sonic jet a little higher than that of the Mach 2.44 jets at $\dot{m}_j = 0.05$ and 0.10 lb_m/s (Figs. 11a and 12a). Higher heat flux at low flow rates is consistent with the findings of Grimaud and McRee [10], as well as Stadler and Inouye [2], who reported an increase in the convective heat transfer up to 100% at low counterflowing jet flow rates. It may be that the LPM jet is (nearly) fully expanded and simply does not have as much cooling effect toward the rim of the model as the underexpanded jets. The decrease in heat flux shows an almost linear trend with increasing flow rate of the counterflowing jet (Fig. 11a) and approaches a minimum value asymptotically (Figs. 11b and 11c). A slight upward trend is seen after reaching the minimum (Fig. 12).

For the underexpanded SPM jets ($\dot{m}_j \geq 0.25$ lb_m/s), the heat flux is seen to be negative, indicating that the flow wetting the model face or forebody cooled the model instead of the shock-induced heating that the model would otherwise experience. The heat flux gauge manufacturer was consulted to assess the validity and uncertainty of the data, as the gauges were not calibrated for negative heat flux. Medtherm advised that, because the calibration was linear, the negative values were expected to be correct, though the uncertainty could be up to $\pm 10\%$, instead of about $\pm 3\%$ for the positive heat flux measurements for which the gauges were calibrated. Such an effect could have a significant application in augmenting traditional or passive TPS to significantly reduce the risk associated with the harsh aerothermal environment at entry and reentry into planetary atmospheres. Negative heat flux, as obtained in these tests, has also been reported in previous work [11,59].

Figure 13 shows a plot of the shock standoff distance Δ, normalized by the diameter of the model versus the flow rate for the 0.5-in.-diam nozzles with design exit Mach numbers of 1.0, 2.44, and 2.94 for the Mach 3.48 freestream interactions. The shock standoff distance increases almost linearly with the jet flow rate, as well as with the design jet nozzle exit Mach number for $\dot{m}_j \geq 0.25$ lb_m/s. The trend is the same for the Mach 4.0 freestream. The figure shows a significant increase in the shock standoff distance of about a factor of 4, compared to the case with no jet injection, indicating much weaker shock strength. The broken lines in the figure are used to connect the data at $\dot{m}_j = 0.25$ lb_m/s to the baseline value. However, for $\dot{m}_j \leq 0.1$ lb_m/s, the broken lines also represent the undefined shock standoff distance for the LPM jets, due to the severe dispersion or lack of definition of the bow shock in the classical sense.

VIII. Numerical Results

The CFD computations were all pretest analyses to enable assessment of some key parameters for the run matrix of the wind-tunnel tests. As such, some test conditions were not used in the pretest

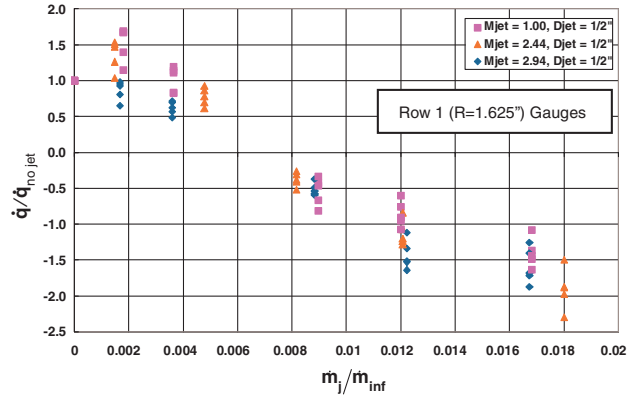

a)

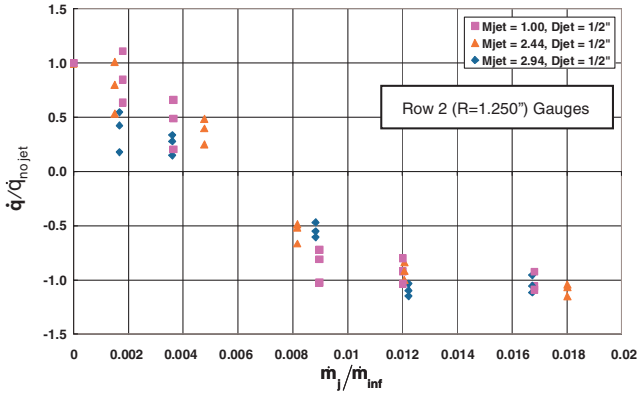

b)

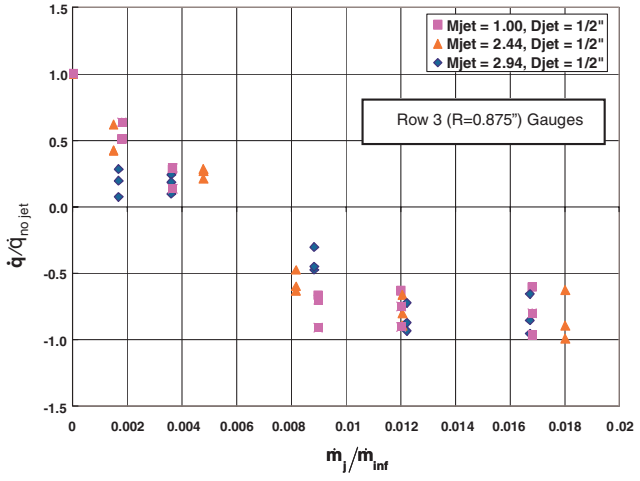

c)

Fig. 11 Variation of heat flux with mass flow rate, $M_{inf} = 3.48$.

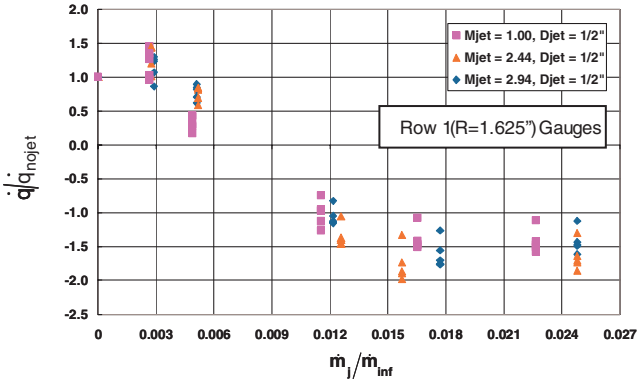

a)

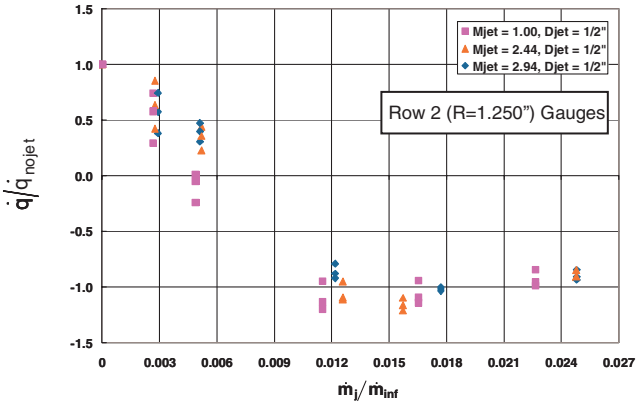

b)

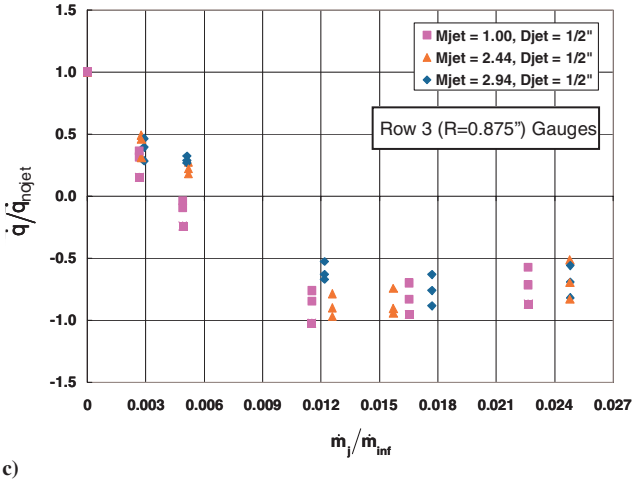

c)

Fig. 12 Variation of heat flux with mass flow rate, $M_{inf} = 4.0$.

CFD solutions. Thus, the CFD solutions were not intended for code validation/benchmarking, in terms of rigorous comparisons between the CFD predictions and the test data for such complex flowfields.

A large number of pretest computations were performed. Here, we present only the solution for the interaction of the Mach 3.48 freestream and the 0.5-in.-diam jet nozzle with design Mach number of 2.94. Snapshots of the computed Mach number, pressure, and temperature distributions of this flowfield are shown in Fig. 14. In general, the CFD predictions give good qualitative agreement with the schlieren images in Figs. 6 and 10. The exception is the $\dot{m}_j = 0.05$ lb_m/s case for which the CFD solutions indicate that the stagnation pressure of the jet was not high enough to produce enough jet momentum to establish either a sustained LPM or SPM flow structure in the Mach 3.48 freestream. However, for the Mach 4.0 freestream, an LPM jet flowfield was well established at $\dot{m}_j = 0.05$ lb_m/s because of the slightly lower freestream static pressure.

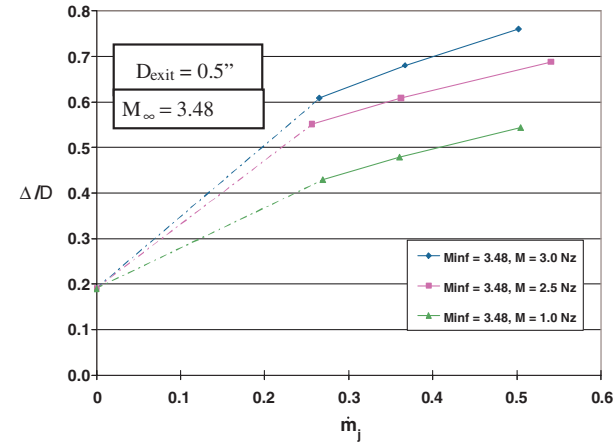

Fig. 13 Shock standoff distance vs mass flow rate.

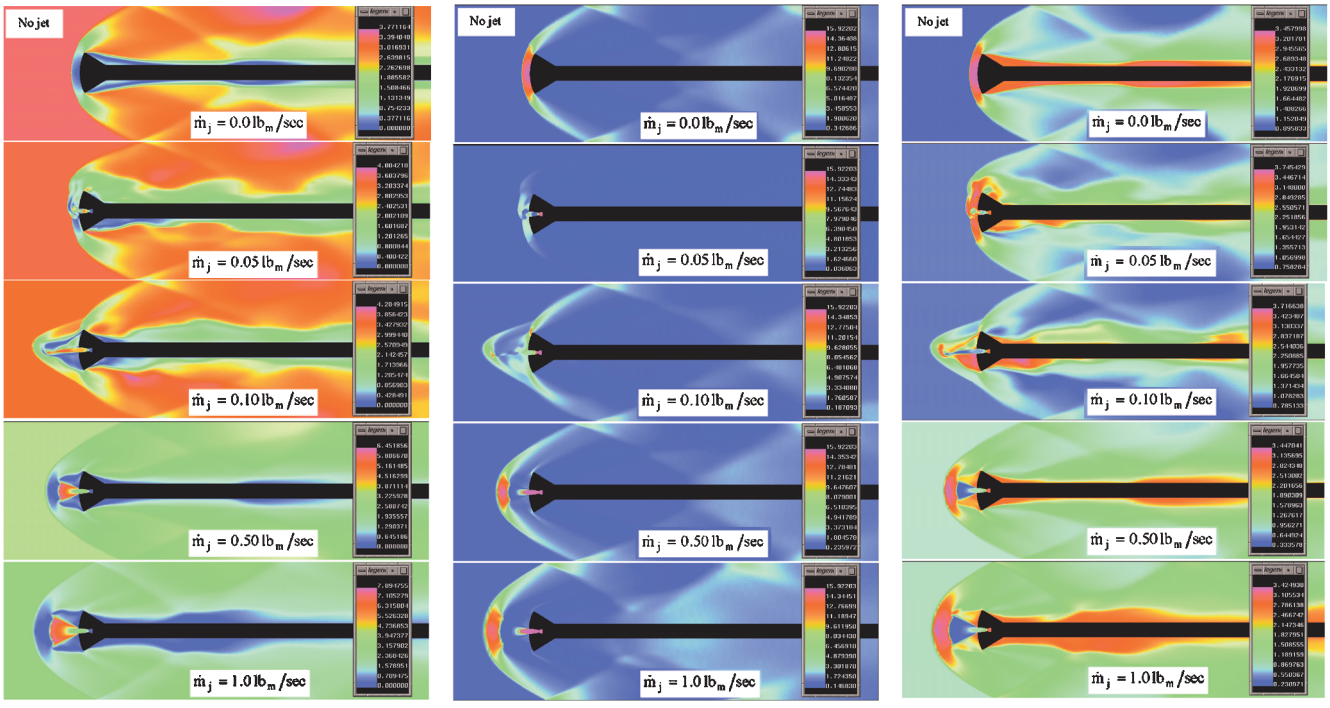

Fig. 14 Predicted flow structure of the interaction of a Mach 3.48 freestream and Mach 2.94 counterflowing jet at different flow rates.

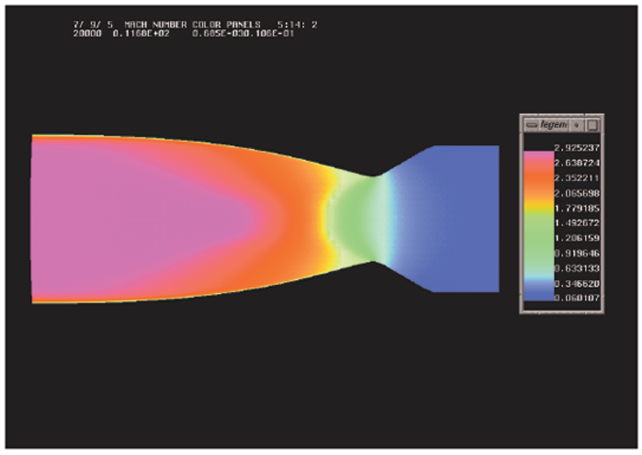

Fig. 15 Mach number distribution of design Mach number of 2.94 nozzle.

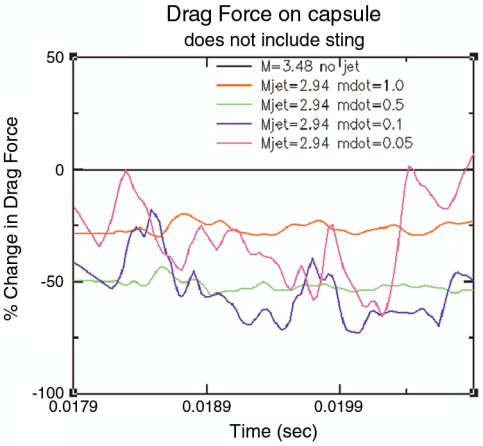

Fig. 16 Change in drag with time.

The LPM jet is quite evident for $\dot{m}_j = 0.10$ lb$_m$/s and it is asymmetric due to the pronounced characteristic unsteadiness and oscillations discussed previously. As the flow rate increased, the structure of the flowfield changed to the SPM jet, showing a clear difference from LPM to SPM. The CFD solutions also show the SPM flow structure to be more steady, though with some degree of

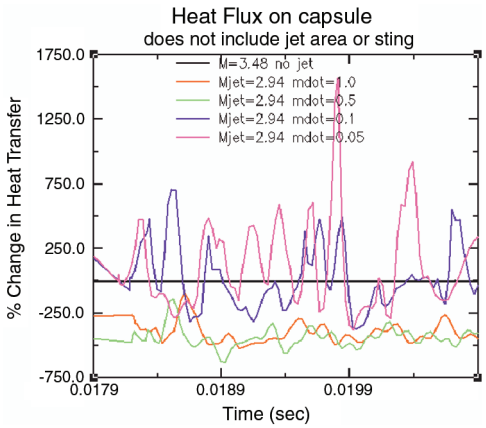

Fig. 17 Change in heat flux with time.

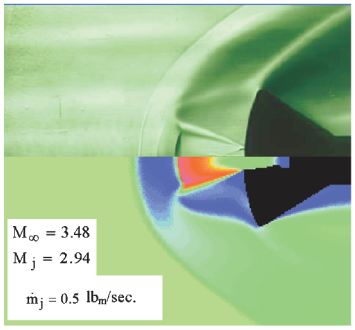

Fig. 18 Comparison of schlieren data with CFD solution (Mach number).

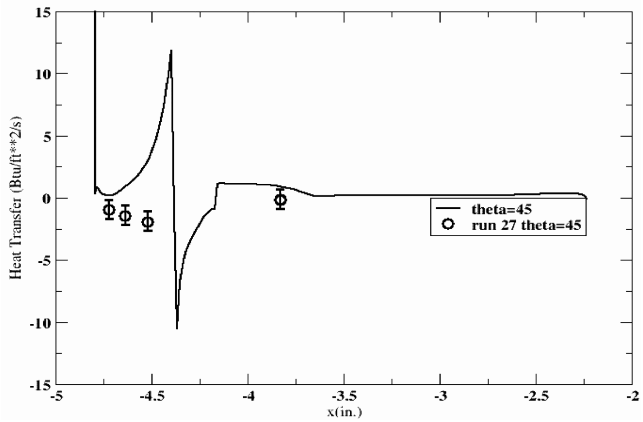

Fig. 19 Comparison of experimental and CFD surface heat transfer.

asymmetry, and consistent with the schlieren data. The pretest analysis enabled the determination of flow rates that would produce an LPM jet and were validated by the test results.

Computations were also performed for the isolated supersonic jet nozzles to determine the quality of the nozzle design. The solution for the nozzle with design exit Mach number of 2.94 is shown in Fig. 15. The CFD solution predicted an exit Mach number of 2.925, giving just a 0.51% difference.

Figures 16 and 17 show the plots of the reduction in the predicted drag and integrated heat flux on the model for the different flow rates. Figure 16 shows a significant reduction in drag, better than 50%, depending on the flow rate, which is generally consistent with the reductions reported in the literature. Figure 17 is the plot of the percentage change in the integrated heat flux for the model for the same nozzle in the Mach 3.48 freestream flowfield. At low jet flow rates, the heat flux varied widely due to the unsteadiness, with spikes that are considerably larger than the baseline value. However, for the SPM jets with flow rates of $\dot{m}_j = 0.5$ and 1.0 lb_m/s, the CFD solutions also predict negative heat flux, and thus are consistent with the experimental data, with a percentage reduction of about 500. Figure 18 shows a qualitative comparison of the CFD prediction and the schlieren data of the interaction between the Mach 3.48 freestream and Mach 2.94 jet at a flow rate of 0.5 lb_m/s. The comparison shows excellent agreement.

The comparison of the experimental heat transfer data and the CFD prediction along the ray, $\theta = 45$ deg, on the face of the model for the same flowfield is shown in Fig. 19. Only four heat flux gauges were placed along that ray (axially), which was insufficient to define a trend in the experimental data. Because there were too few heat flux data to define a trend particularly about the face of the model, it is difficult to infer the agreement or lack of between the data and the prediction. The rise in CFD prediction is due to the impingement of the jet stream at the edge of the model [7], as seen in Fig. 18. However, the values of the predictions and the data are quite comparable.

IX. Summary

Experiments and computational analyses were performed to investigate the potential benefits of an innovative active flow control concept, using counterflowing jets to modify external flowfields and strongly weaken or disperse shock waves around spacecraft in supersonic and hypersonic flows to significantly reduce aerothermal loads and wave drag. The test model was a 2.6%-scale Apollo capsule, designed with interchangeable counterflowing jet nozzle inserts. Five nozzles (three sonic and two supersonic with design Mach numbers of 2.44 and 2.94, exit diameters of 0.25, 0.375, and 0.5 in., and flow rates of 0.05, 0.10, 0.25, 0.35, and 0.50 lb_m/s) were used in two supersonic freestreams of Mach 3.48 and 4.0. The tests were run at three angles of attack (+5, 0, and −9 deg). Pretest CFD analyses were conducted to assess the critical parameters of the freestream-counterflowing interactions. A schlieren system was used to visualize the flowfield and capture the resulting flow structure and shock interactions.

Schlieren data show that these interactions gave an LPM jet at low jet flow rates of 0.05 and 0.1 lb_m/s, whereas the SPM jet was observed at flow rates greater than 0.1 lb_m/s. The LPM and SPM flow structures are very consistent with pretest CFD predictions, qualitatively. The LPM jet is almost fully expanded, creating an interaction in which the bow shock is highly diffused or dispersed into striations of isolated compression waves (as shown in the high-speed camera schlieren data), with very unsteady and oscillatory flow structure. The degree of shock dispersion could have several practical implications, such as sonic boom mitigation, improvement in aerodynamic performance (L/D), and the mitigation of the entropy layer in hypersonic blunt body flows. The heat transfer results also show significant reductions in heat flux, even giving negative heat flux for most of the SPM interactions, which could be significant for spacecraft TPS development for planetary atmospheric entry and reentry.

X. Conclusions

These results strongly suggest that applying active flow control in the form of counterflowing jets can have a strong impact on supersonic and hypersonic vehicle design and performance, such as augmenting passive TPS to significantly reduce the high risks associated with planetary atmospheric entry and reentry. The counterflowing jets appear to be quite effective, even at angles of attack up to 9 deg.

One goal of this work was to advance the state-of-the-art and technology readiness level for counterflowing jets applied as a viable active control technology by gaining a better insight of the flow physics. We believe that this goal has been accomplished based upon the new findings from our tests and CFD analysis.

Acknowledgments

Funding for this study was provided by Vernotto McMillan, Manager of the Innovative Partnership Program Office at NASA George C. Marshall Space Flight Center. Authors Daso and Pritchett also wish to thank Robert Williams, Rebecca Farr, Richard Norman, Henry Brewster, and other coworkers at the Marshall Space Flight Center Experimental Fluids and Environmental Test Branch for persistence, encouragement, and invaluable support in planning and conducting these tests. Authors Daso and Wang express their sincere gratitude to Joe Ruf of the Marshall Space Flight Center Thermal and Combustion Analysis Branch for generating the counterflowing jet nozzle contours using the ADAPT code. The authors also thank William Crosby and Susan Hessler of the Jacobs Engineering, Science, and Technical Services Group for their assistance.

References

[1] Lopatoff, M., "Wing-Flow Study of Pressure-Drag Reduction at Transonic Speed by Projecting a Jet of Air from the Nose of a Prolate Spheroid of Fineness Ratio of 6," NACA RM L51E09, Oct. 1951.

[2] Stadler, J. R., and Inouye, M., "A Method of Reducing Heat Transfer to Blunt Bodies by Air Injection," NACA RM A56B27a, May 1956.

[3] Rashis, B., "Preliminary Indications of the Cooling Achieved by Injecting Water Upstream from the Stagnation Point of Hemispherical, 80° Conical, and Flat-Faced Nose Shapes at a Stagnation Temperature of 4000°F," NACA RM L57103, Oct. 1957.

[4] Ferri, A., and Bloom, M. H., "Cooling by Jets Directed Upstream in Hypersonic Flow," Wright Air Development Center TN 56-382, Sept. 1957.

[5] Resler, E. L., Jr., and Sears, W. R., "The Prospects for Magneto-Aerodynamics," *Journal of the Aeronautical Sciences*, Vol. 25, April 1958, pp. 235–245.

[6] Ziemer, R. W., "Experimental Investigation of Magnetoaerodynamics," *ARS Journal*, Vol. 19, Sept. 1959, pp. 642–646.

[7] Warren, C. H. E., "An Experimental Investigation of the Effect of Ejecting a Coolant Gas at the Nose of a Bluff Body," *Journal of Fluid Mechanics*, Vol. 8, Pt. 3, 1960, pp. 400–417. doi:10.1017/S0022112060000694

[8] Charczenco, N., and Hennessey, K. W., "Investigation of a Retrorocket

Exhausting from the Nose of a Blunt Body into a Supersonic Free Stream," NASA TN D-751, 1961.
[9] Romeo, D. J., and Sterrett, J. R., "Exploratory Investigation of the Effect of a Forward-Facing Jet on the Bow Shock of a Blunt Body in a Mach 6 Free Stream," NASA TN D-1605, 1963.
[10] Grimaud, J. E., and McRee, L. C., "Experimental Data on Stagnation-Point Gas Injection Cooling on Hemispherical-Cone in a Hypersonic Arc Tunnel," NASA TM X-983, July 1964.
[11] Beckwith, I. E., and Bushnell, D. M., "Effect of Intermittent Water Injection on Aerodynamic Heating of a Sphere-Cone at Flight Velocities to 18000 Feet Per Second," NASA TM X-1128, 1965.
[12] Romeo, D. J., and Sterrett, J. R., "Flowfield for Sonic Jet Exhausting Counter to Hypersonic Mainstream," *AIAA Journal*, Vol. 3, No. 3, 1965, pp. 544–546.
doi:10.2514/3.2907
[13] Barber, E. A., "Experimental Investigation of Stagnation Point Injection," *Journal of Spacecraft and Rockets*, Vol. 2, No. 5, 1965, pp. 770–774.
doi:10.2514/3.28277
[14] Finley, P. J., "The Flow of a Jet from a Body Opposing a Supersonic Free Stream," *Journal of Fluid Mechanics*, Vol. 26, Pt. 2, 1966, pp. 337–368.
doi:10.1017/S0022112066001277
[15] Keyes, J. W., and Hefner, J. N., "Effects of Forward-Facing Jets on Aerodynamic Characteristics of Blunt Configuration at Mach 6," *Journal of Spacecraft and Rockets*, Vol. 4, No. 4, April 1967, pp. 533–534.
doi:10.2514/3.28900
[16] Bushnell, D. M., and Huffman, J. K., "Forward Penetration of Liquid Water and Liquid Nitrogen from the Orifice at the Stagnation Point of a Hemispherically Blunted Body in Hypersonic Flow," NASA TM X-1493, March 1968.
[17] Jarvinen, P. O., and Adams, R. H., "The Effects of Retrorockets on the Aerodynamic Characteristics of Conical Aeroshell Planetary Entry Vehicles," AIAA Paper 70-219, Jan. 1970.
[18] McGhee, R. J., "Effects of a Retrorockets Located at the Apex of a 140° Blunt Cone at Mach Numbers of 3.00, 4.50, and 6.00," NASA TN D-6002, Jan. 1971.
[19] Grenich, A. F., and Woods, W. C., "Flow Field Investigation of Atmospheric Braking for High Drag Vehicles with Facing Jets," AIAA Paper 81-0293, Jan. 1981.
[20] *Workshop on Weakly Ionized Gases Proceedings*, Vols. 1, 2 USAF Academy, Colorado, June 1997.
[21] Mishin, G. I., "Experimental Investigation of the Flight of a Sphere in Weakly Ionized Air," AIAA Paper 97-2298, June 1997.
[22] Ghaniev, Yu. CH., Gordeev, V. P., Krasilnikov, A. V., Lagutin, V. I., and Otmennikov, V. N., "Experimental Study of the Possibility of Reducing Aerodynamic Drag by Employing Plasma Injection," *3rd International Congress on Experimental Fluid Mechanics*, Central Research Inst. of Machine Building, Russian Space Agency , and Central AeroHydrodynamic Inst., June 1997.
[23] *2nd Weakly Ionized Gases Workshop Proceedings*, AIAA, Reston, VA, April 1998.
[24] *3rd Weakly Ionized Gases Workshop Proceedings Collocated with the 9th International Space Planes and Hypersonic Systems and Technologies Conference*, AIAA, Reston, VA, Nov. 1999.
[25] Ghaniev, Yu. CH., Gordeev, V. P., Krasilnikov, A. V., Lagutin, V. I., Otmennikov, V. N., and Panasenko, A. V., "Theoretical and Experimental Study of the Possibility of Reducing Aerodynamic Drag by Employing Plasma Injection," AIAA Paper 99-0603, Jan. 1999.
[26] Klimov, A., Leonov, S., Pashina, A., Skvortov, V., Cain, T., and Timofeev, B., "Influence of a Corona Discharge on the Supersonic Drag of an Axisymmetric Body," AIAA Paper 99-4856, Nov. 1999.
[27] Chernyi, G. G., "Some Recent Results in Aerodynamic Applications of Flow with Localized Heat Addition," AIAA Paper 99-4819, Nov. 1999.
[28] Ganguly, B. N., Bletzinger, P., and Garscadden, A., "Shock Wave Damping and Dispersion in Nonequilibrium Low Pressure Argon Plasmas," *Physics Letters A*, Vol. 230, Nos. 3–4, 1997, pp. 218–222.
doi:10.1016/S0375-9601(97)00255-7
[29] Lowry, H., Stepanek, C., Crosswy, L., Sherrouse, P., Smith, M., Price, L., Ruyten, W., and Felderman, J., "Shock Structure of a Spherical Projective in Weakly Ionized Air," AIAA Paper 99-0600, Jan. 1999.
[30] Lowry, H., Smith, M., Sherrouse, P., Felderman, J., Drakes, J., Bauer, M., Pruitt, D., and Keefer, D., "Ballistic Range Tests in Weakly Ionized Argon," AIAA Paper 99-4822, Nov. 1999.
[31] Van Wie, D. M., Wesner, A. L., and Gauthier, L. R., "Shock Wave Characteristics Measured in Gas Discharges," AIAA Paper 99-4824, Nov. 1999.
[32] Kunhardt, E., Saeks, R., Mankowski, J., and Suchomel, C., "One Dimensional Shock Characteristics in Weakly Ionized Gases," AIAA Paper 99-4941, Nov. 1999.
[33] Beaulieu, W., Bytyurin, V., Klimov, A., Leonov, S., Pashina, A., and Timofeev, B., "Plasma Aerodynamic Wind Tunnel Tests With 1/6 Scale Model of Nose Part of F-15," AIAA Paper 99-4825, Nov. 1999.
[34] Malmuth, N. D., Formin, V. M., Maslov, A. A., Fomichev, V. P., Shashkin, A. P., Korotaeva, T. A., Shiplyuk, A. N., and Pozdnyakov, G. A., "Influence of Counterflow Jet on Supersonic Blunt-Body Pressures," AIAA Paper 99-4883, Nov. 1999.
[35] Formin, V. M., Maslov, A. A., Malmuth, N. D., Fomichev, V. P., Shashkin, A. P., Korotaeva, T. A., Shiplyuk, A. N., and Pozdnyakov, G. A., "Influence of Counterflow Jet on Supersonic Blunt-Body Pressures," *AIAA Journal*, Vol. 40, No. 6, June 2002, pp. 1170–1177.
doi:10.2514/2.1768
[36] Shang, J. S., Hayes, J., Wurtzler, K., and Strang, W., "Jet Spike Bifurcation in High Speed Flows," *AIAA Journal*, Vol. 39, No. 6, June 2001, pp. 1159–1165.
doi:10.2514/2.1430
[37] Shang, J. S., Hayes, J., and Menart, J., "Hypersonic Flow Over a Blunt Body with Plasma Injection," AIAA Paper 2001-0344, Jan. 2001.
[38] Shang, J. S., Hayes, J., Miller, J., and Menart, J., "Blunt Body in Electromagnetic Hypersonic Flow Field," AIAA Paper 2001-2803, June 2001.
[39] Shang, J. S., "Plasma Injection for Hypersonic Blunt-Body Drag Reduction," *AIAA Journal*, Vol. 40, No. 6, June 2002, pp. 1178–1186.
doi:10.2514/2.1769
[40] Josyula, E., Pinney, M., and Blake, W., "Applications of a Counterflow Drag Reduction Technique in High Speed Systems," AIAA Paper 2001-2437, June 2001.
[41] Gilinsky, M., Washington, C., Blankson, I. M., Shvets, A. I., "Spike-Nosed Bodies and Forward Injected Jets in Supersonic Flow," AIAA Paper 2002-3918, 2002.
[42] Daso, E. O., Beaulieu, W., Hager, J. O., "Prediction of Drag Reduction in Supersonic and Hypersonic Flows with Counter-Flow Jets," AIAA Paper 2002-5115, 2002.
[43] Woods, W. C., Jones, K. M., and Genzel, N. N., "Preliminary Investigation of the Effect of Stagnation Point Liquid Injection on the Aerothermodynamics of Blunt Bodies,'' AIAA Paper 2002-15-2, 2002.
[44] Hayashi, K., Aso, S., and Tani, T., "Numerical Study of Thermal Protection by Opposing Jets," AIAA Paper 2005-188, Jan. 2005.
[45] Cook, D. R., "14-Inch Wind Tunnel Schlieren System," NASA Marshall Space Flight Center, Aerodynamics Division, Electro-mechanical Branch, WTN-105, Jan. 1964.
[46] Smith, S. D., "Aerospike Design and Performance Tool: ADAPT Upgrades and Enhancements," Plumetech Final Rept. PT-FR-04-03, June 2004.
[47] Chakravarthy, S. R., Szema, K. Y., Haney, J. W., "Unified 'Nose-to-Tail' Computational Method for Hypersonic Vehicle Applications," AIAA Paper 88-2564, 1988.
[48] Ota, D. K., Chakravarthy, S. R., Darling, J. C., "An Equilibrium Air Navier–Stokes Code for Hypersonic Flows," AIAA Paper 88-0419, Jan. 1988.
[49] Palaniswany, S., Ota, D. K., Charavarthy, S. R., "Some Reacting-Flow Validation Results for USA-Series Codes," AIAA Paper 91-0583, Jan. 1991.
[50] Rockwell, D., and Naudascher, E., "Self-Sustained Oscillations of Impinging Shear Layers," *Annual Review of Fluid Mechanics*, Vol. 11, Jan. 1979, pp. 67–94.
doi:10.1146/annurev.fl.11.010179.000435
[51] Panaras, A. G., "Pulsating Flows About Axisymmetric Concave Bodies," *AIAA Journal*, Vol. 19, No. 6, 1981, pp. 804–806.
doi:10.2514/3.7816
[52] Suzuki, H., Kasagi N., and Suzuki, Y., "Active Control of an Axisymmetric Jet with Distributed Electromagnetic Flap Actuators," *Experiments in Fluids*, Vol. 36, No. 3, 2004, pp. 498–509.
doi:10.1007/s00348-003-0756-0
[53] Edney, B. E., "The Effects of Shock Impingement on the Heat Transfer Around Blunt Bodies at $M = 4.6$ and 7," AIAA Paper 66-756, Sept. 1966.
[54] Edney, B. E., "Effects of Shock Impingement on the Heat Transfer around Blunt Bodies," *AIAA Journal*, Vol. 6, No. 1, Jan. 1968, pp. 15–21.
doi:10.2514/3.4435
[55] Wieting, A. R., "Multiple Shock–Shock Interference on a Cylindrical Leading Edge, *AIAA Journal*, Vol. 30, No. 8, Aug. 1992, pp. 2073–2079.
doi:10.2514/3.11181
[56] Albertson, C. W., and Venkat, V. S., "Shock Interaction Control For

Scramjet Cowl Leading Edges," AIAA Paper 2005-3289, 2005.
[57] Heckman, D., Lahaye, C., Moir, L., Podesto, B., and Robertson, W., "A Shock Wave Attenuation Treatment for Ballistic Ranges," *AIAA Journal*, Vol. 8, No. 7, July 1970, pp. 1355–1357.
[58] Suzuki, K., Himeki, H., Watanuki, T., and Abe, T., "Experimental Studies on Characteristics of Shock Wave Propagation Through Cylinder Array," Inst. of Space and Astronautical Science No. 676, March 2000.
[59] McMahon, H. M., "An Experimental Study of the Effect of Mass Injection at the Stagnation Point of a Blunt Body," Ph.D. Thesis, California Inst. of Technology, Pasadena, CA, 1958.

E. Gutmark
Associate Editor